Sensors & Actuators: B. Chemical 282 (2019) 580–589

Contents lists available at ScienceDirect

Sensors and Actuators B: Chemical

journal homepage: www.elsevier.com/locate/snb

Anti-myeloma activity and molecular logic operation by Natural Killer cells in microfluidic droplets

Saheli Sarkar[a], Seamus McKenney[a], Pooja Sabhachandani[a], James Adler[b], Xiaozhe Hu[b], Dina Stroopinksy[c], Jacalyn Rosenblatt[c], David Avigan[c], Tania Konry[a,*]

[a] Department of Pharmaceutical Sciences, Northeastern University, 360 Huntington Avenue, Boston, MA, 02115, USA
[b] Department of Mathematics, School of Arts and Sciences, Tufts University, Medford, MA 02155, USA
[c] Beth Israel Deaconess Medical Center, Harvard Medical School, Boston, MA 02115, USA

ARTICLE INFO

Keywords:
Single cell analysis
Microfluidics
Nanoliter droplets
Dynamic imaging
Agent-based model

ABSTRACT

Immune-targeted therapies that activate effector lymphocytes such as Natural Killer (NK) cells are currently being investigated for the treatment of Multiple myeloma (MM), the second most common form of hematological cancer. However, individual NK cells are highly heterogeneous in their cytolytic potential, making it difficult to detect, quantify and correlate the outcome of dynamic effector-target cell interactions at single cell resolution. Here, we present a microfluidic bioassay platform capable of activity-based screening of cellular and molecular immunotherapies. We identified distinct functional signatures associated with NK-MM cell interaction. The addition of immunomodulatory drug lenalidomide altered responses of NK-susceptible MM cells but not that of NK-tolerant MM cells. Antitumor cytotoxicity was significantly increased by the blockade of PD1/PDL1 axis as well as the clinically relevant cell line NK92, which were used to construct molecular logic functions (AND and NOT gates). A predictive agent-based mathematical model was developed to simulate progressive disease states and drug efficacy. The findings of the current study validate the applicability of this microfluidic cytotoxicity assay for immunotherapy screening, biocomputation and for future employment in detection of patient-specific cell response for precision medicine.

1. Introduction

Immunotherapy is widely considered to be the new frontier of anti-cancer treatment strategies. While immunotherapy has shown promising results against certain types of solid tumors (e.g., melanoma, colorectal), it is particularly suitable against hematological malignancies as the immune and cancer cells are present in the same environment, increasing the likelihood of immune-mediated anti-cancer activity [1,2]. Cancer cells, however, develop various approaches to evade immune surveillance, including the expression of immune checkpoint pathways such as Programmed Death 1 (PD-1). A number of molecular (e.g., monoclonal antibody, antibody drug conjugates, bispecific T cell engagers) and cellular immunotherapies (chimeric antigen receptor (CAR)–T and Natural Killer (NK) cells) have been implemented or are currently under investigation in clinical trials. Several such approaches have been specifically designed for patients affected with multiple myeloma (MM), the second most common type of hematologic malignancy [3]. This includes immunomodulatory drugs (IMiDs) like lenalidomide, immune checkpoint inhibitors like anti-PD1/PDL1 antibodies and genetically modified targeted effector lymphocytes (T/NK cells). MM remains incurable despite the application of several types of therapeutic approaches. Furthermore, many patients are prone to relapse or develop therapeutic resistance over time, in which case single agents can be used in combination to increase their efficacy [4,5]. Understanding the mechanism of interaction between the MM targets and immunotherapies as well as the potency and efficacy of drugs *a priori* would facilitate streamlining treatment options for personalized medicine. However, at present, it is not feasible to assess MM cell responses prior to the drug treatment so as to obtain predictive insights into the expected outcome.

One of the primary mechanisms by which immunotherapies act against MM is to enhance activation of NK cells, increase NK-mediated interaction, antibody-dependent cellular cytotoxicity and upregulate FasL and Granzyme B expressions in NK cells [3,5]. Therefore, a quantitative *in vitro* model of drug cytotoxicity for MM should allow characterization of the interaction between NK and MM cells during immune-targeted therapeutic screening. The experimental model should take into consideration the phenotypic and functional

* Corresponding author.
E-mail address: t.konry@northeastern.edu (T. Konry).

https://doi.org/10.1016/j.snb.2018.11.068
Received 15 September 2018; Received in revised form 2 November 2018; Accepted 13 November 2018
Available online 17 November 2018

heterogeneity of NK cells since the cytolytic potential of NK cells varies widely [6]. NK cell-mediated cytotoxicity is also known to be dependent on effector to target (E-T) cell ratios. Utilizing high E-T ratios, as often done in conventional cytotoxicity assays, to detect target death in a short time period may not simulate physiological cell ratios appropriately [7]. NK cells are also known to conjugate with and detach from target cells rapidly and variably, which cannot be determined by endpoint assays. Therefore, monitoring NK-target cell interaction at E-T ratios of ≤ 1:1 in a sensitive, dynamic assay can inform us of the characteristics and potency of single effector cells. This is better achieved by employing microscale sensors and molecular devices capable of assessing single cell functions such as migration, activation, differentiation and secretion [8–10]. While the interaction of activated NK cells with model NK-responsive target cell lines have been analyzed at single cell resolution [11–13], the efficacy of MM-targeted immunotherapies or the anti-myeloma activity of NK cells has not been investigated at single cell level.

We have previously reported a microfluidic droplet-based cytotoxicity assay that permits stable co-encapsulation and time-lapse imaging of heterotypic cells at 1: 1 E-T ratio [14]. In this paper, we propose a combined experimental and computational drug screening approach for determining the efficiency of NK-mediated cellular (clinically relevant NK-92 line) and molecular immunotherapies (lenalidomide, anti-PDL1 antibody) against MM. The quantitative results from discrete NK-MM cell interaction in droplets were used to develop an agent-based mathematical model of single NK cell lytic interaction with a target cell. Incorporating the expression of PD-1/PD-L1 axis in this model, we simulated progressive disease states indicated by increasing levels of PD-1 and PD-L1 and assessed inhibition of the pathway with anti-PD-1 drugs.

The cytolytic potential of NK cells provides an ideal opportunity to perform Boolean logical operations due to the evident binary output of the experimental system, i.e., kill (death of target cells) or no kill (survival of target cell) using fluorescent viability indicators. The presence or absence of small molecule or antibody-based drugs further enhance the response of the model by activating/inhibiting specific signaling pathways and promoting NK cell cytotoxicity. Various proteins, enzymes, antigens, antibodies, DNA and RNA have been used previously to design molecular logic gates in the field of biomolecular computing [15–20]. The logic gates are primarily implemented with bacterial cells; there are fewer examples of utilizing mammalian cell functions to realize logic operations [21–23]. Here, we detected an AND functionality using single NK-target cell interactions in the presence of anti-PD-L1 antibody, which significantly increased NK cell cytotoxicity. We further show that the high levels of cytotoxicity exhibited by the NK-92 cells demonstrate inverter or NOT gate in this platform. These results are the first step towards building complex whole cell biomolecular computational systems by leveraging single cell-based biosensing approaches.

2. Materials and methods

2.1. Microfluidic device fabrication and droplet generation

The microfluidic devices were fabricated by standard soft-lithography protocols [14,24]. Briefly, the microfluidic design was etched on silicon wafers with a negative photo resist SU-8 2100 (MicroChem, Newton, MA) to obtain features of 150 μm height. Poly(dimethylsiloxane) (PDMS) (Sylgard 184, Dow Corning, Midland, MI) devices were prepared by mixing the pre-polymer with silicone elastomer curing agent at 10:1 ratio (w/w) and poured over the wafer. The mixture was degassed and cured for 12 h at 65 °C. Individual PDMS devices were peeled from the wafer, bonded to microscope slides by heating at 90 °C for 10 min. Each inlet of the device was connected to individual syringes containing aqueous (i.e., cell suspension in media) or oil-based fluids through Tygon Micro Bore PVC tubing (0.010" ID, 0.030" OD, 0.010" wall, Small Parts Inc., FL, USA). The device was treated with Aquapel glass treatment (Aquapel, Pittsburg, USA) for 15 min, then flushed with air immediately before experiments. The syringes were operated by individually programmable syringe pumps (Harvard Apparatus, USA). To obtain optimal droplet sizes the oil to aqueous flow rates were generally maintained at a ratio of 4:1 in the device. The oil phase consisted of Fluorinert® FC-40 (Sigma, St. Louis, MO) supplemented with 2% w/w surfactant (008-FluoroSurfactant, Ran Biotechnologies, Beverly, MA).

2.2. Cell isolation and culture

RPMI-8226 (multiple myeloma (MM) cell line) was purchased from American Type Culture Collection (ATCC, Manassas, VA) and maintained in RPMI-1640 medium supplemented with 10% Fetal Bovine Serum and 1% Antibiotic-Antimycotic solution (Corning Cellgro, Manassas, VA). NK-92 cells were obtained from Nantkwest Inc (Woburn, MA) and maintained in X-Vivo 10 media (Lonza, NJ) supplemented with 5% human serum and 500 IU/mL IL-2 (ProSpec Bio, East Brunswick, NJ). All cells were grown at 37 °C under 5% CO_2 in a humidified atmosphere. Cells were routinely passaged every three days and harvested at a density of 1×10^6 viable cells/mL.

Primary human NK cells were sorted via FACS from peripheral blood of a healthy donor by labeling PBMCs with FITC-conjugated CD56 antibody (BD Biosciences, San Jose, CA). Freshly isolated cells were maintained in RPMI-1640 media containing 10% FBS, 1% antibiotic and 100 U/mL IL-2 (Roche Diagnostics, Indianapolis, IN).

2.3. Activation of NK cells and NK-mediated cytolysis in droplets

RPMI-8226 cells were labeled with 2μM Calcein AM off-chip for 30 min at 37 °C as per manufacturer's instructions (Live/Dead Viability/Cytotoxicity assay, Life Technologies, Carlsbad, CA). The labeled cells were washed and loaded in a syringe at an initial concentration of 1.25 million/ mL. Unlabeled $CD56^+$ NK cells were loaded in a separate syringe at same concentration for co-encapsulation in droplets. Prior to PD-L1 blockade experiments, RPMI-8226 cells were pretreated with 500 U/mL Interferon gamma (IFN-γ, R&D Systems) for 24 h [25] and subsequently incubated with anti-PD-L1 blocking antibody (BPS Bioscience, San Diego, CA) for 24 h. Lenalidomide was dissolved in DMSO as per manufacturer's instructions (Sigma Aldrich, St. Louis, MO). It was diluted in media to 2.3μM immediately prior to use [26]. The treated RPMI-8226 cells were mixed with lenalidomide in the syringe and loaded in the microfluidic device following similar procedure as stated above.

2.4. Image acquisition, processing and statistical analysis

The phase/fluorescent images of cells in droplets were captured using Zeiss Axio Observer.Z1 Microscope (Zeiss, Germany) equipped with a Hamamatsu digital camera C10600 Orca-R2 and 1 0-4 0× objectives. The excitation/emission wavelengths of Calcein AM are 494/517 nm and were imaged using standard FITC filters. The microfluidic device containing cell-encapsulated droplets was maintained in a humidified microscopic stage-top incubator at 37 °C and 5% CO_2 for the duration of the experiment. All time-lapse images were obtained by automated software control. The array was scanned to identify locations containing 1:1 effector: target ratio and the specific x-, y-, and z-positions were programmed in the Zen imaging program (Zeiss). Images of these locations were obtained every 5 min for a total period of 5 h using LD Plan-Neofluar 20x/0.4 Corr Ph2 objective (Zeiss). Image processing and analysis was done with ImageJ (http://rsb.info.nih.gov/ij/), Microsoft Office Excel 2010, and Origin Pro software. The proportion of dead cells was calculated as a ratio of the number of dead cells to the total number of cells and expressed as 'Death (%)'. Fluorescent intensity of the cells at every time point was analyzed by

selecting the region of interest (i.e., the cell body) and measuring mean intensity in ImageJ. Normalized fluorescent intensity (NFI) for each cell was calculated as a ratio of fluorescent intensity at every time point with respect to fluorescent intensity at the initial time. NK-mediated cytolysis of target cells was characterized by decrease of ≥80% in NFI due to the loss of calcein AM from target cells [14]. All periods of association (visible E-T conjugation) and dissociation (non-contact) between NK and target cells were analyzed for each cell to determine the number of contacts undergone by each cell pair. Killing time for contact-dependent target death was defined as the time elapsed from the initiation of contact to loss of fluorescence. All statistical analysis was performed using non-parametric two-sided Mann Whitney U test, and p value < 0.05 was considered statistically significant.

2.5. Modeling NK contact dynamics

To model single-cell interaction, we coupled agent-based model (ABM) paradigm with a Monte Carlo simulation, averaging the results over several interactions. More details about the model and simulation parameters have been provided in Supporting Information. The entire model was implemented using Matlab©.

3. Results and discussion

3.1. Dynamic features of NK cell conjugation and target cytolysis

MM cells have been shown to be susceptible to NK-mediated cytolysis in population-averaged assays [27,28]. Here, individual primary $CD56^+$ NK cells were co-encapsulated with single RPMI-8226 target cells in microfluidic droplets. The high density droplet docking array was designed to accommodate 56 droplets per mm^2 and allows trapping of 4000 droplets per experiment (Fig. S1 A,B). The droplet dimensions were maintained at radii of 45 ± 5 μm and volumes of 380–523 pL. Co-encapsulation of heterotypic cell pairs in these droplets follows Poisson probability, resulting in droplets containing 0–4 cells of each type as well as blank droplets. To reliably measure target-NK cell interaction and subsequent cytolysis at single cell level, we monitored droplets containing E-T cell ratio of 1:1 for up to 5 h (Fig. 1A,B).

Co-encapsulation of primary NK cells obtained from healthy volunteers resulted in increased RPMI-8226 cell death in droplets (12 ± 4% compared to 1 ± 1% spontaneous RPMI-8226 death, p value 0.05) (Fig. 1C). MM cell death occurred primarily due to contact-mediated mechanisms since encapsulation of MM cells in NK cell-conditioned media, collected from IL2-treated and untreated NK cells, did not change death rates (Fig. 1D). Contact-independent target killing appears to be cell-type specific, as primary lymphoma cells and cell lines were killed without direct contact in microfluidic droplets in our previous study [14]. Leukemia cells were also killed by NK cell-secreted exosomes in non-microfluidic assays [29].

The different phases of dynamic interaction between NK and MM targets, as observed in microfluidic droplets, are outlined in Fig. 1A. NK cells initially depict motility towards the MM cells (Fig. S2 A) and show morphological changes, including cell elongation and uropod formation during conjugation (Fig. 1B). Overall, we observed that large numbers of E-T cell pairs established at least one contact in three independent experiments (n = 101, 129 and 106 pairs respectively) (Fig. 1E-F). Following immune complex formation with the target, some NK cells remained conjugated until target cell lysis (Fig. 1B). However, in two out of three experiments, over 75% of the complexes detached and the NK cell moved away before the target cell underwent lytic death (Fig. S2B). Multiple contacts (2–10) occurred between these cell pairs, lasting anywhere from 5 to 250 minutes (Fig. 1E). The total duration of target cell conjugation was varied not only in each experiment but across experiments (average values: 132, 97 and 183 min; Fig. 1F).

Some of the contacts observed in droplets could be considered a transient “scanning” motion between NK and target cells instead of stable synaptic conjugation (Fig. 1A). Here, we separated the contact periods of cells undergoing multiple contacts into initial contact periods (TI) and final contact periods (TF; Fig.1G). The final contacts were significantly longer than the initial contacts in all cases, suggesting that stable contacts occurred following initial scanning of target cell surfaces ($p < 0.01$-0.0001, Fig. 1G).

Cytolytic lymphocytes can kill multiple target cells sequentially [30]. We observed NK cells making contact with 2–4 target cells at a frequency of 21 ± 5% out of 148 cell pairs (Movie S1, Movie S2). There was no difference in total contact duration or death times between the one-to-one and one-to-many kills. However, we did not assess serial killing extensively since the primary goal was to monitor cytolysis at E:T ratio of 1:1.

Functional analysis of primary NK cell interaction with target cells have been performed previously in microwells, which accommodate up to 50 cells, and nanowells, which restrict occupancy to 4 cells [11,12]. The findings of these studies suggest significant differences in NK cell cytotoxic capacity, migratory behavior and phases of interaction. IL-2-treated NK cells were shown to form > 1 contacts [13]. Variability in contact duration and conjugation has been observed with different cell lines as targets [12,13]. *In vivo* contacts formed between NK cells and tumor cells were shown to be largely transient (up to 10 min); *in vitro* analysis with non-cancer cells suggested longer contact durations (~100 min) [12,31]. Our results also demonstrate similar heterogeneity at single cell level. While it may be challenging to measure time-varying interaction of two types of suspension cells (effector and target) in many macro- and micro-scale platforms, it was robustly achieved in droplets for long periods without physical restraints (e.g., traps, weirs) or adhesive ligands (e.g., antibodies). This makes the platform suitable for investigating both stable and transient interactions between various types of immune cells and target cells as well as relevant biological events including multiple target killing [24,32]. Serial killer NK cells have the ability to kill 4 or more targets within 16 h [30,33,34]. Onfelt and colleagues reported that 20% of the NK cell population are serial killers, forming 4–8 conjugates over a 12 h time period [12]. The scope of this study was to investigate MM cell killing at 1:1 E-T ratio in droplets, but it is possible to investigate serial killing by encapsulating > 1 target cells in droplets by increasing the initial density of target cell suspension.

3.2. Increased cytolytic potential of NK-92 cells

Since primary NK cells did not kill RPMI-8226 cells with high efficiency, we determined the efficacy of an established NK cell line NK92 against these targets (Fig. 2A). Herein, co-encapsulation of NK92 cells with RPMI-8226 cells resulted in markedly higher target cell death (Fig. 2B). In contrast to the variability observed in primary NK cells, NK92 cells predominantly formed single contacts with target cells (Fig. 2C). The total contact duration of cells forming single contacts lasted for significantly shorter period compared to cells forming multiple contacts (average values: 28 vs. 82 min, $p < 0.0001$, Fig. 2D). The death of target cells that required multiple contacts occurred at delayed time in comparison with single-contact cells (average values: 29 vs. 112 min, $p < 0.0001$, Fig. 2E). The correlation between total contact duration and time to death was higher (0.9) for cells requiring single contact compared to cells requiring 2–3 contacts (0.8-0.7). Given the strong correlation between the two parameters, it is evident that even short contacts with NK92 cells were sufficient to induce death in target cells.

In contrast with primary NK cells, NK92 cells showed shorter contact periods with target cells (average duration of 137 min vs. 46 min respectively) and required significantly less time to kill targets ($p < 0.05$, Fig. 2F). Four fold higher number of NK92 cells remained conjugated with MM cells at the time of death (NK92: 31 ± 2%, primary NK: 7 ± 6%). We further assessed the efficacy of effector cell activity by measuring the time required for NK cells to find the targets

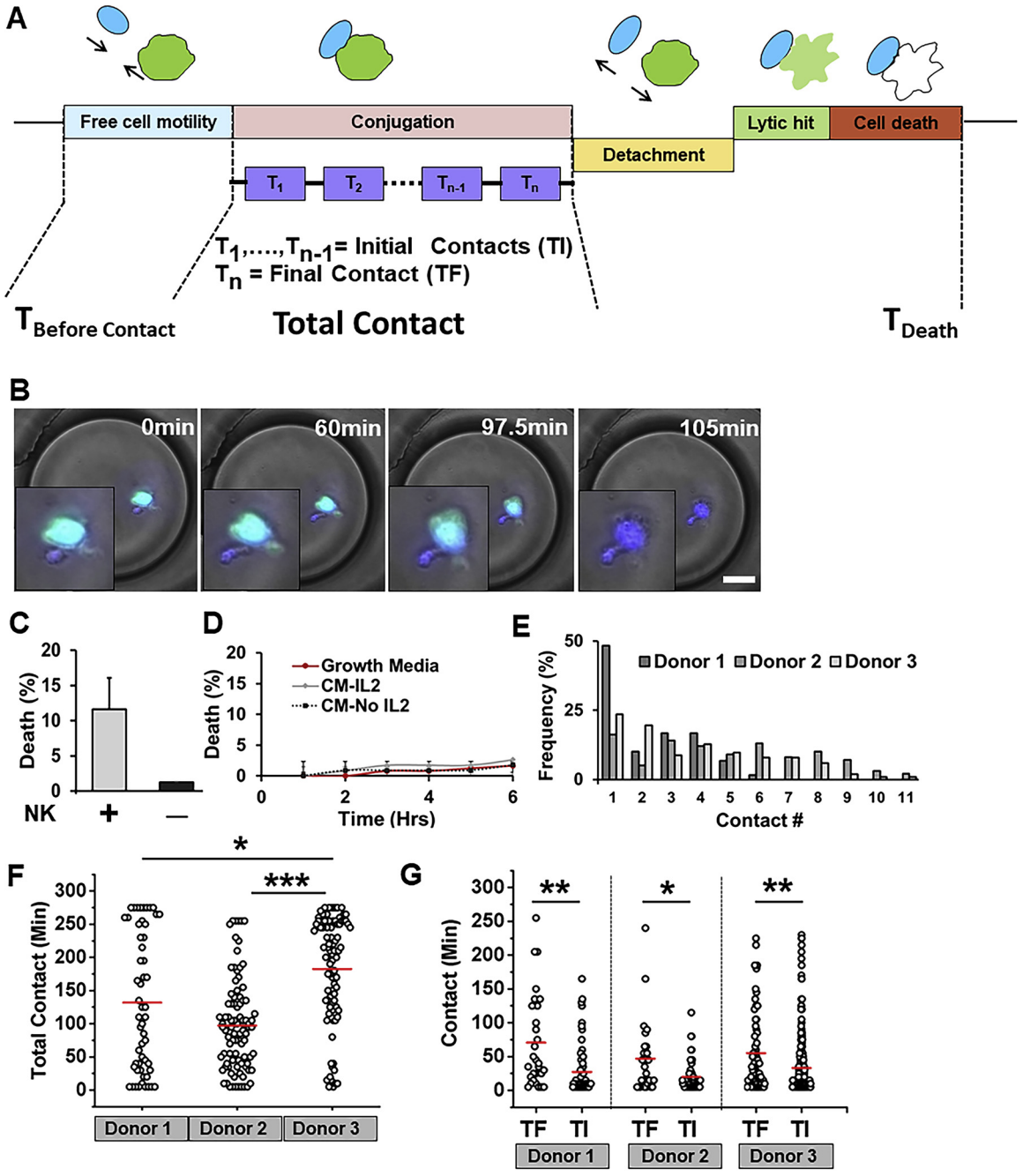

Fig. 1. Cytolysis of MM cells in microfluidic droplets. (A) Annotation of parameters identifying the various interactive phases in droplets: NK and target cells move freely in droplets before conjugation (Time (T) $_{\text{Before Contact}}$) ; Conjugation (Total Contact) between each NK-MM cell pair, which may occur once or multiple times throughout experimental period; Occasional detachment of cell pairs before death; and death (indicated by loss of fluorescence; T_{Death}). Total Contact is defined as the sum of all contacts between the same cell pair. For cells that undergo multiple contacts, Final Contact (TF) is defined by the last, stable conjugation period while previous contacts are referred as Initial Contacts (TI). (B) Representative image of RPMI-8226 cell labeled with Calcein AM (green) and Hoechst (blue) and NK cell labeled with Hoechst interacting in droplet. Cell death occurs at 105 min. Scale bar: 20 μm. (C) Death of RPMI-8226 cells in droplets. Data is represented as Mean ± SEM of three independent replicates. (D) RPMI-8226 cell death in droplets in the presence of conditioned media (CM) obtained from IL-2-treated (CM-IL2) or untreated (CM-No IL2) NK cells. (E) Frequency of contacts between RPMI-8226 cells and NK cells obtained from three separate donors. N = 101, 129 and 106 NK cells were assessed respectively. (F) Total contact durations between NK-RPMI-8226 cells. * indicates p value < 0.01; *** indicates < 0.00001. (G) Duration of final contacts (TF) and initial contacts (TI) for cell pairs that demonstrated multiple contacts in droplets. * indicates p value < 0.01; ** indicates < 0.0001 (For interpretation of the references to colour in this figure legend, the reader is referred to the web version of this article).

in droplets and form conjugates. NK92 cells formed conjugates faster than primary NK cells (average 9 vs. 25 min, $p < 0.0001$) (Fig. 2G). Thus, NK92 cells outperformed primary NK cells in all quantitative criteria in the droplets, exhibiting greater cytotoxicity against RPMI-8226 cells.

NK92 cells have been shown to recognize and kill multiple target cells in preclinical models and have yielded promising results in phase I clinical trials against solid tumors (renal cell and lung cancer) and hematological malignancies [35,36]. NK-92 cells efficiently killed bulk and clonogenic MM cells [37]. The findings from our microfluidic bioassay are thus in accordance with these reports and raise the possibility that NK92 cells can be effective against MM in a clinical setting.

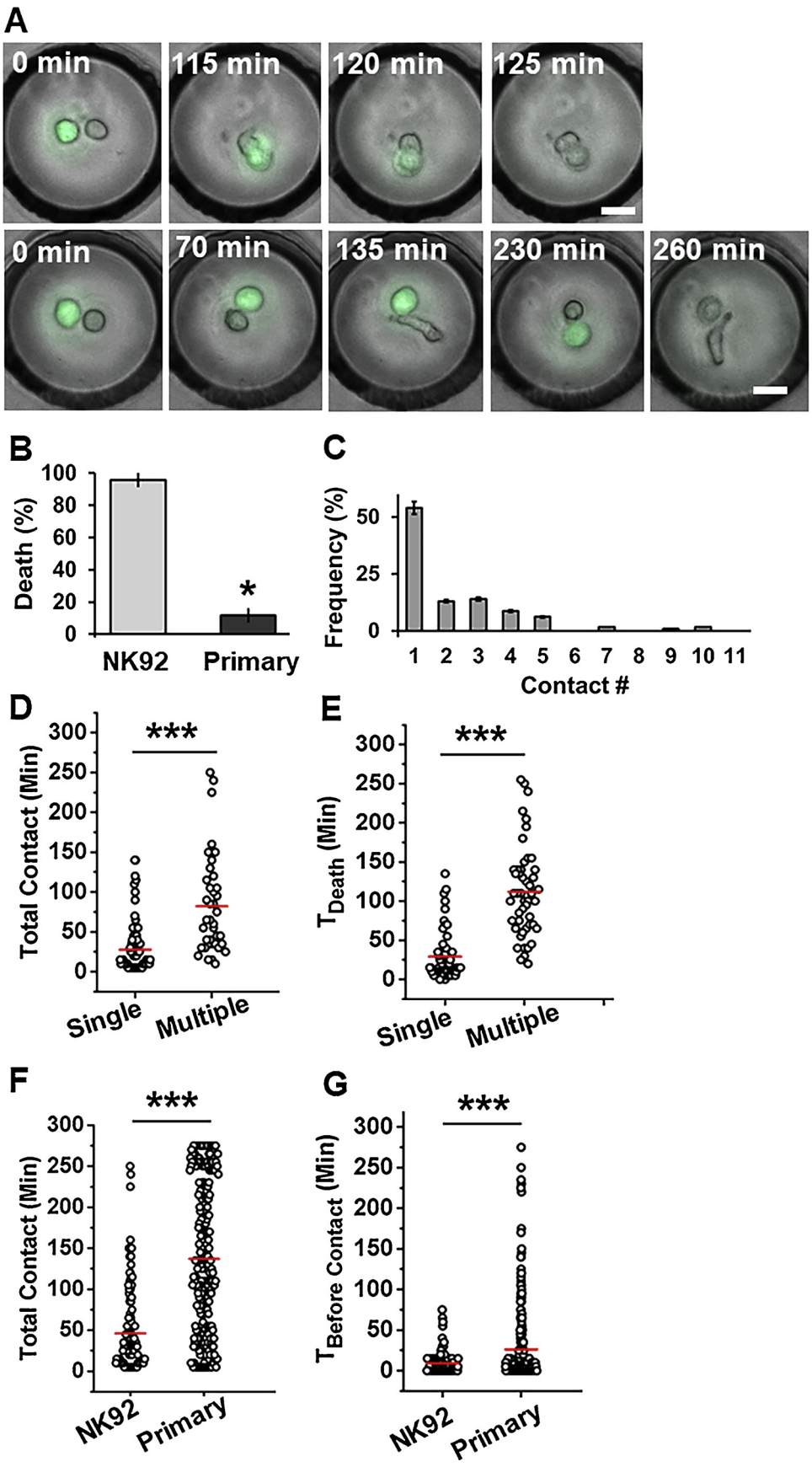

Fig. 2. Quantification of NK-92 cell interaction with RPMI-8226 cells in droplets. (A) Representative images of unlabeled NK cells interacting with, and killing, RPMI-8226 cells labeled with Calcein AM (green) in droplet. Scale bar: 20 μm. (B) Death of RPMI-8226 cells mediated by NK92 cells (n = 139 cell pairs) or primary NK cells (n = 336 cell pairs) in droplets. Data indicates mean ± SEM. (C) Frequency of contacts between RPMI-8226 cells and NK92 cells. (D) Total contact duration for RPMI-8226 cells that made single or multiple contacts with NK92 cells. (E) Time of death for MM cells that made single or multiple contacts with NK92 cells. (F) Comparing contacts made by all RPMI-8226 cells with NK92 and primary NK cells. (G) Time preceding conjugation of RPMI-8226 cells with NK92 and primary NK cells. *** $p < 0.0001$ (For interpretation of the references to colour in this figure legend, the reader is referred to the web version of this article).

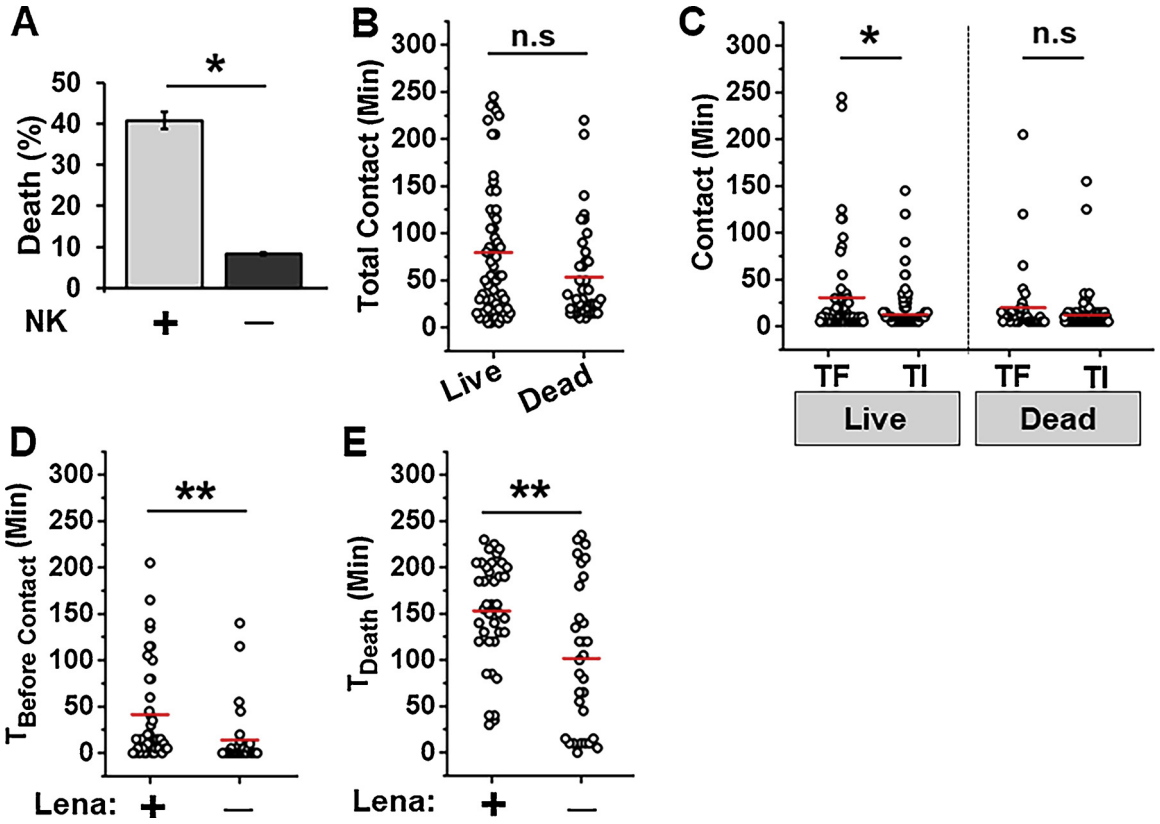

Fig. 3. Effect of lenalidomide treatment in droplets. (A) Death of RPMI-8226 cells mediated by primary NK cells in the presence (n = 144 cells) or absence (n = 384 cells) of lenalidomide. Data indicates mean ± SEM. (B) Comparing total contact duration made by lenalidomide-treated primary NK cells with RPMI-8226 cells. (C) Duration of final contacts (TF) and initial contacts (TI) for cell pairs that demonstrated multiple contacts. * $p < 0.01$. (D) Time preceding conjugation of RPMI-8226 cells with primary NK cells prior to cell death. (E) Time of death in droplets. ** $p < 0.001$.

3.3. Increasing primary NK cell cytotoxicity with lenalidomide

We next assessed the feasibility of screening different types of therapeutic agents, including small molecule drugs and antibody-based inhibitors, using our analytical approach. Here we determined the effect of lenalidomide, a small molecule derivative of thalidomide, in modifying the efficacy of NK cell activity in droplets [26]. This drug is known to activate T and NK cells and improve recognition of malignant cells by NK cells [5,38]. Lenalidomide increased spontaneous death of RPMI-8226 cells in droplets (8 ± 1% vs. 1 ± 1% in untreated cells). It increased the cytotoxic potential of primary NK cells significantly (41 ± 2% vs. 12 ± 4%, $p < 0.05$, Fig. 3A). The target cells killed by lenalidomide-treated NK cells depicted contacts of similar duration compared to the cells that survived (Fig. 3B), thus suggesting that the decision to kill a target cell is not solely dependent on the duration of contact between the effector and target cell. In a standard end-point assay, it is not possible to determine whether the cells that survived did so due to a lack of contact with NK cells; the droplet-based dynamic monitoring approach allowed us to rule out this possibility.

We further probed the cell subsets that survived and cells that died to extract specific functional features and compared them to untreated cells. First, considering the cells that were not killed by NK cells, we found that initial contacts were shorter than the final contacts (average of 12 and 31 min, $p < 0.01$, Fig. 3C). This trend was also observed in control cells (Fig. 1G). However, lenalidomide treatment eliminated significant differences in the initial (average: 12 min) and final (20 min) contacts of target cells that died, although this trend was detected in the untreated NK-mediated dead cell subgroup (Fig. 3C). The time required to find target cells and establish contact was significantly higher in case of the lenalidomide-treated NK cells ($p < 0.001$) (Fig. 3D). Concomitant to this finding, target cell death occurred at a later time in the lenalidomide-treated subgroup compared to the untreated control cells ($p < 0.001$) (Fig. 3E). Thus, the droplet-based bioassay facilitated detection of common trends in the observed functional features from untreated control group to drug-treated subgroup, and further helped validate the functional cytotoxicity analysis at single cell level.

3.4. Analyzing the effect of checkpoint blockade inhibitor in droplet bioassay

We also investigated the role of another pertinent immunomodulatory agent, the check-point inhibitor PD-L1, in NK-mediated MM cell death [27]. RPMI-8226 were found to express PD-L1, which was further upregulated by treated with IFN-γ (Fig. 4A). We pre-treated RPMI-8226 cells with an anti-PD-L1 blocking antibody and observed a significant increase in target cell death ($p < 0.001$, Fig. 4B). However, blockade of the PD-L1 pathway did not change the basic interactive characteristics of target cells (Fig. 4C). The total contact times, death times and time required for effector cells to home in on target cells did not differ between PD-L1-treated and untreated cell groups. It was not possible to compare live cells between these two groups as few target cells survived the PD-L1 blockade. Within the PD-L1 treated cells, we found no difference between the overall contact times of cells that made single contact and those making multiple contacts (Fig. 4D). This is unlike NK92 cells, where multiple contacts occurred over longer periods (Fig. 2D). However, similar to NK92 cells, there was a significant delay ($p < 0.001$) in the death of PD-L1 treated target cells that made multiple contacts with NK cells (Fig. 4E).

Recent evidence indicates that the NK cells of some otherwise healthy individuals may also express PD-1, possibly due to latent infection [39]. $CD56^+$ $CD3^-$ NK cells isolated from healthy donors can be induced to express PD-1 after IL-2 treatment, while PD-1 expression is

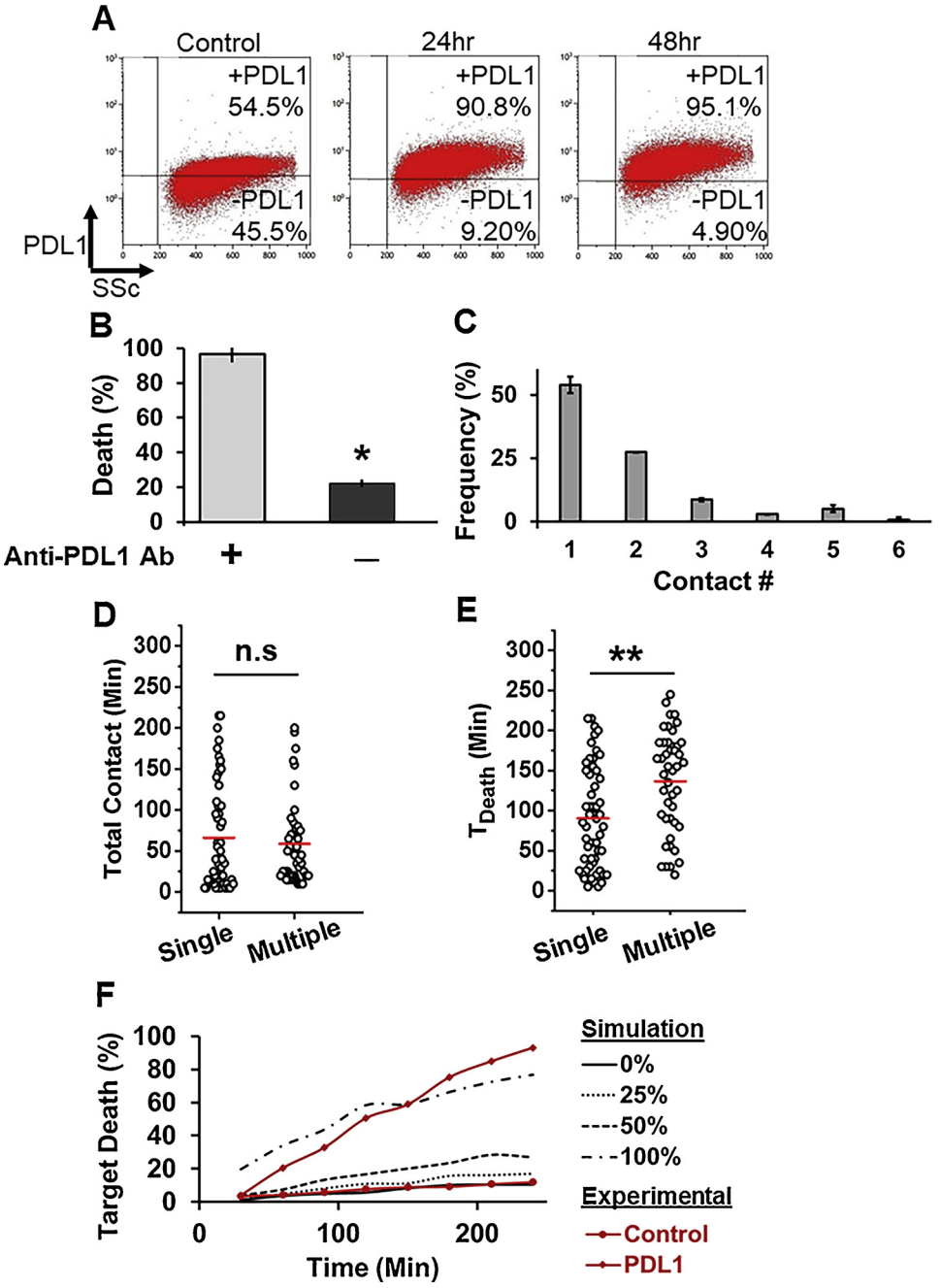

Fig. 4. Blockade of PD1/PDL1 axis in droplets. (A) PD-L1 expression in RPMI-8226 cells measured by flow cytometry. Cells were treated with IFN-γ for 24 and 48 h. (B) Death of RPMI-8226 cells mediated by primary NK cells in the presence (n = 230 cells) or absence (n = 336 cells) of ani-PDL1 antibody. Data indicates mean ± SEM. (C) Frequency of contacts between RPMI-8226 cells and primary NK cells. (D) Duration of contact made by anti-PD-L1 antibody-treated RPMI-8226 cells with primary NK cells. Cell pairs are separated into two categories based on the number (single or multiple) of contacts made. (E) Time of target cell death in droplets. ** $p < 0.001$. (F) Comparing simulation (black lines) with experimental data (red lines). At 0% drug efficiency (i.e., no PD-L1 drug), NK cell populations expressing PD1 minimally kill MM cells expressing PDL1. Increasing the efficiency of drug binding to 25, 50 and 100% show gradual increases in MM cell death. Cumulative data from single-cell experiments (from Fig. 1C and Fig. 4B) was summed and plotted over time (For interpretation of the references to colour in this figure legend, the reader is referred to the web version of this article).

upregulated in NK cells from MM patients [28]. Myeloma cell lines such as U266 and human MM cells express PD-L1 [25]. PD-1 has been shown to inhibit cytotoxicity, granule exocytosis and secretion of IFN-γ by NK cells. Blocking PD-1 with a novel monoclonal anti-PD-1 antibody resulted in increased cell migration, Granzyme and IFN-γ secretion and cytotoxicity [28]. Blocking PD-L1 with anti-PD-L1 antibody also increased survival of mice implanted with myeloma [40]. The increased cytotoxicity against MM cells due to blocking of PD-L1 in droplets validate the findings in current literature and suggest that this platform can be used to determine the efficacy of immunotherapies accurately.

3.5. Computational analysis of individual NK cell function

We further employed a combination of experimental and mathematical techniques to model the effect of PD-1/PDL1 pathway on NK cell functionality. Based on the variability in lytic interaction between NK and target cells in droplets, we developed an agent based model (ABM) to simulate the dynamics of contact-mediated cytolysis by individual cells (Fig. S3 A). We incorporated a Monte Carlo-type simulation to average the results to get more meaningful data [44]. To simulate the model with varying proportion of cells expressing PD-1 and PD-L1, we used quantitative data available in current literature. Up to 64% NK cells from multiple myeloma patients have showed expression of PD-1 [28]. Conversely, PD-L1 was increased significantly in plasma cells from MM patients (0%–92% range) compared to no expression in healthy patients [25].

In the absence of anti-PD-L1 antibody, the model simulations show that the dynamic trends of target death are consistent with experimental findings (Control (in red), Fig. 4F). Contact-mediated target death increased over time (1 to 10% by 4 h). It has been argued that there is an inherent delay in NK-mediated target death (5 h), which could be due to the lag time between lytic hit and actual cell death, or due to the necessity of priming NK cells [41]. At single cell level, we observed significant death at ≤60 min in droplets; therefore, we did not

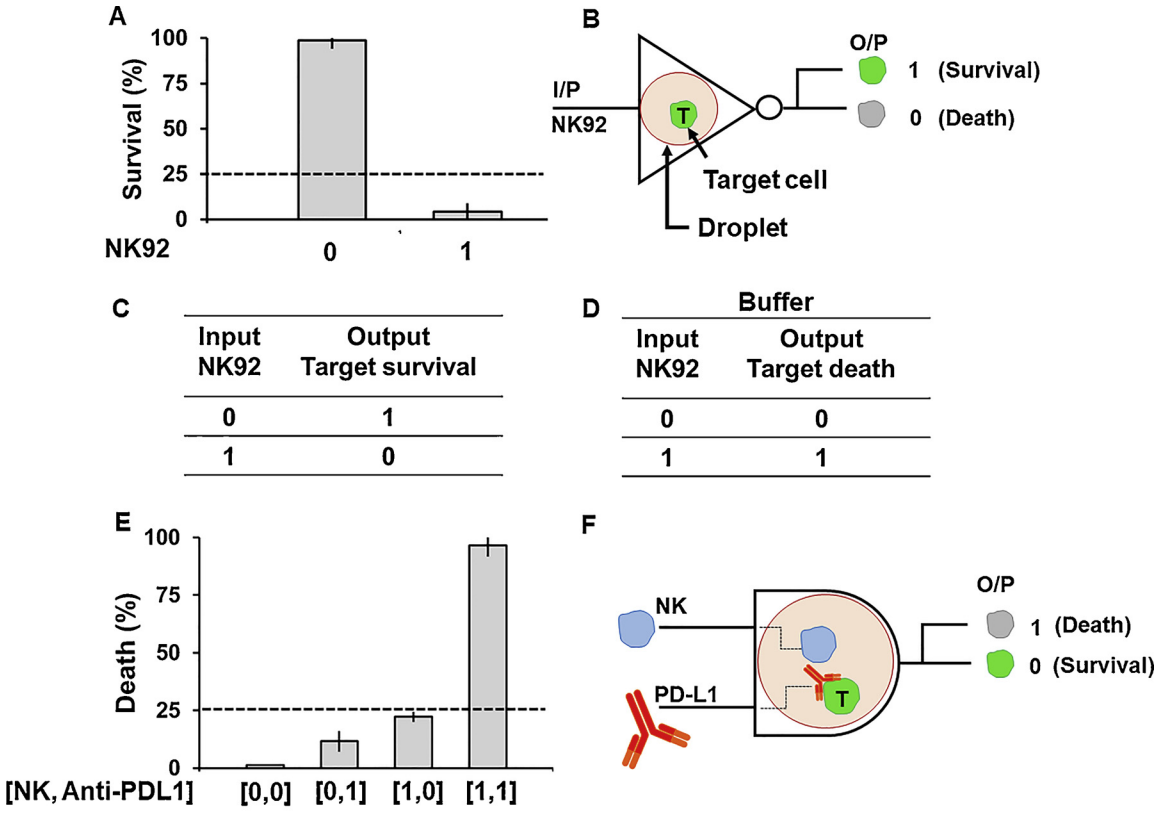

G

Input 1 NK	Input 2 PD-L1	Output Target death
0	0	0 (Low)
0	1	0 (Low)
1	0	0 (Low)
1	1	1 (High)

Fig. 5. Molecular logic operations in droplets. (A–C) NOT gate designed using NK-92 cells as input and target cell survival as output. (A) Survival (%) of target cells in the absence (0) or presence (1) of NK-92 cells. (B) Schematic of NOT gate showing fluorescence output from target cells. (C) Truth table of NOT gate. (D) Buffer function using NK92 cells as input and target cell death as output. (E–G) AND gate function using primary NK cells and anti-PDL1 antibody as inputs and target cell (T) death as output. (E) Quantification of MM cell responses in the presence of PDL1 antibody. The threshold of detection was set at 25% cell death. (F) Schematic of AND gate showing fluorescence output from target cells. (G) Truth table of AND gate using values and threshold as indicated in (E).

include delay time or priming factors in our model. We then modeled the effect of inhibiting the PD-1/PD-L1 pathway with anti-PD-L1 antibody at increasing levels of drug efficacy (E_{max}). As E_{max} increases from 0 to 50%, cytolytic effect of NK cells improves markedly (Fig. 4F). Assuming that the drug operates at maximum efficacy (100%), NK-mediated cytotoxicity increased to 77%. The model-simulated findings match the trends of experimental data obtained with the neutralizing anti-PD-L1 antibody (PDL1 (in red), Fig. 4F).

We subsequently modified this model to characterize varying levels of cytolytic potency of NK cells. Target cell lines shown as susceptible to NK cells, such as K562, Jurkat, Daudi, SUDHL10 etc may be killed at rates ranging from 40 to 95% [14,29,42]. Along this line, NK92 cells were far more effective against RPMI-8226 cells in our study. Therefore, we generalized the model to implicate a wider killing activity and raised the overall baseline cytolytic potential (70–80%). In this situation, increasing PD-1 expression from 1.4% (assumed to be healthy cells) to 50% (advanced MM) did not change target death if there was no corresponding expression of PD-L1 (Fig S3B). As expected, expression of PD-L1 alone while maintaining constant PD-1 expression at 1.4% did not change myeloma death in the model either (Fig S3C). Next we simulated different stages of myeloma progression by assuming variable levels of PD-1^+ and PD-$L1^+$ cells in the NK and myeloma populations respectively. As the results indicate, NK-dependent anti-tumor effect is governed by the extent of both PD-1 and PD-L1 expression as well as drug efficiency (Fig. S4).

Various mathematical models have been developed in the past to analyze and model the immune system. Traditionally, ordinary differential equations (ODEs) are used for modeling population dynamics, for example, delay differential equations (DDEs) and stochastic differential equations (SDEs). We refer to [41,43–45] for more details. In certain cases, spatial effects are also important and cannot be ignored. Partial differential equations (PDEs) have been used to explicitly model the spatial dependence. However, such differential equation-based models were not considered suitable for this single cell study since we are studying individual behaviors and interactions rather than averages of population dynamics. The ABM paradigm is more intuitive and suitable for modeling individuals (agents) and their interactions with other individuals and environment [46–48]. Heterogeneity and stochasticity

are easily added into the ABM. Our model considered two cells and their interactions, which allowed us to focus on the status of the individuals in a more dynamical way. Standard ABMs have the capability to model many agents (cells) and their interactions, usually by a complex network. In future this model can be expanded to address complex biological phenomena (secretion, multiple cell inputs and competing signaling pathways).

3.6. Boolean functions exhibited by NK-target cell interactions

Biological computation and information processing is an emerging field that makes use of analytes and whole cells to accomplish various logical operations and further develop complex networks for different types of biomedical, chemical and environmental applications. Logic gates have been previously constructed using genetic transcriptional circuitry in bacterial colonies but rarely in whole cells. Here, we take a different approach by harnessing the inherent functionality of NK cells to achieve logic operations. As discussed above, NK-92 cells showed high levels of cytotoxicity against MM cells (Fig. 2B). If we consider target cell survival as the output, NK-92 cells perform as a NOT (Inverter) gate (Fig. 5A-C). On the other hand, changing the output variable to target cell death, we find that the absence of NK-92 (i.e., input 0) results in minimal (1%) target death (output 0) while the presence of NK-92 (i.e., input 1) causes 95% target death (≈ output 1). This can be defined as a single input digital Buffer gate, which does not alter the logic relationship between input and output (Fig. 5D). In Boolean simulators, a buffer can be used to increase propagation delay. In this case, the delay induced is 5 h, which is the duration of the experiment. Thus, the natural cytotoxicity of the immune cells served as a biochemical mechanism to yield variable logic responses in the microfluidic droplets.

Primary NK cells can also be used to define logic gate operations in droplets. A two input AND gate was devised by considering primary NK cells and anti-PDL1 antibody as the inputs and MM cell death as the output (Fig. 5E, F). The application of PD-L1 antibody in the absence of NK cells resulted in low % death (output ≈ 0) of target cells (Fig. 4B), while the same was true for primary NK cells in the absence of PD-L1 antibody (Fig. 1C). Only by combining the two inputs could the output be 1 (96% cell death), thereby satisfying the conditions for an AND gate (Fig. 5G). Reversibly, a NAND gate can be implemented with the same inputs and by taking cell survival as a readout. NAND gates are particularly useful since they are one of two universal gates, that is, any other logic gate can be designed by various combinations of this gate. This approach can be further extended with different types of activating and inhibitory reagents to obtain assorted Boolean operations.

In conclusion, the microfluidic droplet array device provides an effective technique to evaluate dynamic cell–cell interactions in MM through functional phenotyping. It is highly beneficial for screening the efficacy of immunomodulatory treatments, and will be complementary to existing bulk analytical tools in revealing heterogeneity in individual cell responses. The experimental platform served as a paradigm, based on single cell reaction toward immunotherapies, for designing whole-cell logic gate operations. It can be employed for molecular biocomputation applications in detecting cell-cell communication, drug responses and personalized diagnostics. Furthermore, by utilizing the experimental data to establish a predictive model, we provide a comprehensive pipeline to investigate and anticipate the outcome of therapeutic application in a given disease model.

Author Contribution

SS, SM and PS designed and conducted microfluidic experiments. JA and XH developed the analytical model. DS isolated and characterized cell populations. SS and SM performed the acquisition, analysis, and interpretation of the data. SS wrote manuscript with inputs from SM, JA, XH and PS. JR, DA and TK substantially contributed to the conception of the work and revised it critically for important intellectual content. All the authors approved the final version of the manuscript.

Acknowledgement

This work was funded by NIH/NCI grant R21 [RM11-014] [to T.K.].

Appendix A. Supplementary data

Supplementary material related to this article can be found, in the online version, at doi:https://doi.org/10.1016/j.snb.2018.11.068.

References

[1] S. Menon, S. Shin, G. Dy, Cancers 8 (2016) 106.
[2] A. Im, S.Z. Pavletic, J. Hematol. Oncol. 10 (2017) 94.
[3] M. Kocoglu, A. Badros, Pharmaceuticals 9 (2016) 3.
[4] G. Görgün, M.K. Samur, K.B. Cowens, S. Paula, G. Bianchi, J.E. Anderson, R.E. White, A. Singh, H. Ohguchi, R. Suzuki, S. Kikuchi, T. Harada, T. Hideshima, T. Yu-Tzu, J.P. Laubach, N. Raje, F. Magrangeas, S. Minvielle, H. Avet-Loiseau, N. Munshi, D.M. Dorfman, P.G. Richardson, K.C. Anderson, Clin. Cancer Res. 21 (2015) 4607–4618.
[5] M. Giuliani, B. Janji, G. Berchem, Oncotarget 8 (2017) 24031.
[6] A. Horowitz, D.M. Strauss-Albee, M. Leipold, J. Kubo, N. Nemat-Gorgani, O.C. Dogan, C.L. Dekker, S. Mackey, H. Maecker, G.E. Swan, Sci. Trans. Med. 5 (2013) 208ra145-208ra145.
[7] F. Cerignoli, Y.A. Abassi, B.J. Lamarche, G. Guenther, D. Santa Ana, D. Guimet, W. Zhang, J. Zhang, B. Xi, PLoS One 13 (2018) e0193498.
[8] M. Kirschbaum, M.S. Jaeger, C. Duschl, Lab Chip 9 (2009) 3517–3525.
[9] Y. Zhou, S. Basu, E. Laue, A.A. Seshia, Biosens. Bioelectron. 81 (2016) 249–258.
[10] X. An, V.G. Sendra, I. Liadi, B. Ramesh, G. Romain, C. Haymaker, M. Martinez-Paniagua, Y. Lu, L.G. Radvanyi, B. Roysam, PLoS One 12 (2017) e0181904.
[11] Y.J. Yamanaka, C.T. Berger, M. Sips, P.C. Cheney, G. Alter, J.C. Love, Integr. Biol. 4 (2012) 1175–1184.
[12] B. Vanherberghen, P.E. Olofsson, E. Forslund, M. Sternberg-Simon, M.A. Khorshidi, S. Pacouret, K. Guldevall, M. Enqvist, K.-J. Malmberg, R. Mehr, Blood 121 (2013) 1326–1334.
[13] P.E. Olofsson, E. Forslund, B. Vanherberghen, K. Chechet, O. Mickelin, A. Rivera Ahlin, T. Everhorn, B. Önfelt, Front. Immunol. 5 (2014) 80.
[14] S. Sarkar, P. Sabhachandani, D. Ravi, S. Potdar, S. Purvey, A. Beheshti, A.M. Evens, T. Konry, Front. Immunol. (2017) 8.
[15] E. Katz, V. Privman, Chem. Soc. Rev. 39 (2010) 1835–1857.
[16] B. Wang, M. Buck, Chem. Commun. (Camb.) 50 (2014) 11642–11644.
[17] A. Tamsir, J.J. Tabor, C.A. Voigt, Nature 469 (2011) 212–215.
[18] W. Weber, R. Schoenmakers, B. Keller, M. Gitzinger, T. Grau, Proc. Natl. Acad. Sci. U. S. A. 105 (2008) 9994–9998.
[19] C. Lou, X. Liu, M. Ni, Y. Huang, Q. Huang, L. Huang, L. Jiang, D. Lu, M. Wang, C. Liu, D. Chen, C. Chen, X. Chen, L. Yang, H. Ma, J. Chen, Q. Ouyang, Mol. Syst. Biol. 6 (2010) 350.
[20] Z. Xie, S.J. Liu, L. Bleris, Y. Benenson, Nucleic Acids Res. 38 (2010) 2692–2701.
[21] W. Weber, M. Fussenegger, Curr. Opin. Chem. Biol. 15 (2011) 414–420.
[22] S. Ausländer, D. Ausländer, M. Müller, M. Wieland, M. Fussenegger, Nature 487 (2012) 123–127.
[23] R. Gaber, T. Lebar, A. Majerle, R. Jerala, Nat. Chem. Biol. 10 (2014) 203–208.
[24] S. Sarkar, P. Sabhachandani, D. Stroopinsky, K. Palmer, N. Cohen, J. Rosenblatt, D. Avigan, T. Konry, Biomicrofluidics 10 (2016) 054115.
[25] J. Liu, A. Hamrouni, D. Wolowiec, V. Coiteux, K. Kuliczkowski, D. Hetuin, A. Saudemont, B. Quesnel, Blood 110 (2007) 296–304.
[26] M.A. Dimopoulos, M. Hussein, A.S. Swern, D. Weber, Leukemia 25 (2011) 1620–1626.
[27] J. Godfrey, D.M. Benson Jr, Leuk. Lymphoma 53 (2012) 1666–1676.
[28] D.M. Benson, C.E. Bakan, A. Mishra, C.C. Hofmeister, Y. Efebera, B. Becknell, R.A. Baiocchi, J. Zhang, J. Yu, M.K. Smith, Blood 116 (2010) 2286–2294.
[29] L. Lugini, S. Cecchetti, V. Huber, F. Luciani, G. Macchia, F. Spadaro, L. Paris, L. Abalsamo, M. Colone, A. Molinari, J. Immunol. 189 (2012) 2833–2842.
[30] R. Bhat, C. Watzl, PLoS One 2 (2007) e326.
[31] J. Deguine, B. Breart, F. Lemaître, J.P. Di Santo, P. Bousso, Immunity 33 (2010) 632–644.
[32] G. Yesiloz, M.S. Boybay, C.L. Ren, Lab Chip 15 (2015) 4008–4019.
[33] S. Isaaz, K. Baetz, K. Olsen, E. Podack, G.M. Griffiths, Eur. J. Immunol. 25 (1071-) (1995) 1079.
[34] J.A. Lopez, A.J. Brennan, J.C. Whisstock, I. Voskoboinik, J.A. Trapani, Trends Immunol. 33 (2012) 406–412.
[35] H. Klingemann, L. Boissel, F. Toneguzzo, Front. Immunol. 7 (2016) 91.
[36] T. Tonn, D. Schwabe, H.G. Klingemann, S. Becker, R. Esser, U. Koehl, M. Suttorp, E. Seifried, O.G. Ottmann, G. Bug, Cytotherapy 15 (2013) 1563–1570.
[37] B.E. Swift, B.A. Williams, Y. Kosaka, X.-h. Wang, J.A. Medin, S. Viswanathan, J. Martinez-Lopez, A. Keating, Haematologica 97 (2012) 1020–1028.
[38] C. Fionda, M.P. Abruzzese, A. Zingoni, F. Cecere, E. Vulpis, G. Peruzzi, A. Soriani, R. Molfetta, R. Paolini, M.R. Ricciardi, Oncotarget 6 (2015) 23609.

[39] S. Pesce, M. Greppi, G. Tabellini, F. Rampinelli, S. Parolini, D. Olive, L. Moretta, A. Moretta, E. Marcenaro, J. Allergy Clin. Immunol. 139 (2017) 335–346 e3.
[40] W.H. Hallett, W. Jing, W.R. Drobyski, B.D. Johnson, Biol. Blood Marrow Transplant. 17 (2011) 1133–1145.
[41] C.R. Almeida, A. Ashkenazi, G. Shahaf, D. Kaplan, D.M. Davis, R. Mehr, PLoS One 6 (2011) e24927.
[42] S.S. Somanchi, K.J. McCulley, A. Somanchi, L.L. Chan, D.A. Lee, PLoS One 10 (2015) e0141074.
[43] L. Kuepfer, M. Peter, U. Sauer, J. Stelling, Nat. Biotechnol. 25 (2007) 1001.
[44] C. Watzl, M. Sternberg-Simon, D. Urlaub, R. Mehr, Front. Immunol. 3 (2012) 359.
[45] K.R. Duffy, P.D. Hodgkin, Trends Cell Biol. 22 (2012) 457–464.
[46] A.K. Chavali, et al., Characterizing emergent properties of immunological systems with multi-cellular rule-based computational modeling, Trends Immunol. 29 (2008) 589–599.
[47] G. Shahaf, M. Barak, N.S. Zuckerman, N. Swerdlin, M. Gorfine, R. Mehr, J. Theor. Biol. 255 (2008) 210–222.
[48] A. Kaplan, S. Kotzer, C.R. Almeida, R. Kohen, G. Halpert, M. Salmon-Divon, K. Köhler, P. Höglund, D.M. Davis, R. Mehr, J. Immunol. 187 (2011) 760–773.